Synthesis, structural and physicochemical properties of a series of manganese(II) complexes with a novel *N*5 tripodal-amidate ligand and their potential use as water oxidation catalysts

Michael G. Papanikolaou[a], Sofia Hadjithoma[b], John K. Gallos[c,*,5], Haralampos N. Miras[d,*,4], John C. Plakatouras[a,e*,3], Anastasios D. Keramidas[b,*,2], Themistoklis A. Kabanos[a,*,1]

[a] *Section of Inorganic and Analytical Chemistry, Department of Chemistry, University of Ioannina, GR 45110 Ioannina, Greece*

[b] *Department of Chemistry, University of Cyprus, 2109 Nicosia, Cyprus*

[c] *Department of Chemistry, Aristotle University of Thessaloniki, Thessaloniki GR 541 24, Greece*

[d] *WestCHEM, School of Chemistry, University of Glasgow, Glasgow G12 8QQ, UK*

[e] *Institute of Materials Science and Computing, University Research Center of Ioannina, Ioannina, GR-45110, Greece*

[*]Corresponding authors.

E-mail addresses: igallos@chem.auth.gr (J.K. Gallos), Charalampos.Moiras@glasgow.ac.uk (H.N. Miras), iplakatu@uoi.gr (J.C. Plakatouras), akeramid@ ucy.ac.cy (A.D. Keramidas), tkampano@uoi.gr (T.A. Kabanos).

[1] ORCID: 0000-0001-6944-5153.

[2] ORCID: 0000-0002-0446-8220.

[3] ORCID: 0000-0003-4665-6593.

[4] ORCID: 0000-00020086-5173.

[5] ORCID: 0000-0002-3732-918X.

Keywords: Manganese, Electrochemistry, X-ray structure

ABSTRACT:

Water oxidation plays a crucial role in both natural and artificial photosynthesis, which is an attractive solution to the depletion of fossil fuels as energy sources due to the increasing consumption. Thus, the search for oxygen evolution reaction catalysts is a hot topic of research. Reaction of the N5-tripodal amidate ligand, *N*-{2-[(bis(pyridine-2-ylmethyl)amino)methyl]phenyl}picolinamide (Htrip) with $M^{II}X_2$ (X = Cl^-, Br^-, I^-), in anhydrous ethyl alcohol, and C_2H_5ONa yields the complexes [Mn^{II}(trip)Cl] (**1**), [Mn^{II}(trip)Br] (**2**), and [Mn^{II}(trip)I] (**3**). Single crystal X-ray structure analysis of **1**-**3** revealed that the manganese(II) atom in the three manganese compounds occupies the center of a distorted octahedral coordination sphere consisting of two pyridine, one picoline and one amino nitrogen atoms on the equatorial plane, while the axial positions are occupied by one amido nitrogen atom and the halogen anion. The three manganese(II) complexes **1**-**3** constitute the first examples of mononuclear {$Mn^{II}(N5_{trip})X$} species to be reported. Magnetic susceptibility measurements showed that these complexes are high-spin d^5 systems. Cyclic voltametric study of **1**-**3** revealed an unexpected two electron, electrochemically reversible redox process, assigned to the oxidation of Mn^{II} to Mn^{IV}. The electrochemical properties for oxygen evolution reaction of complexes **1**-**3** showed that the oxidized $trip^-$ ligand is responsible for the electrocatalytic oxidation of water to dioxygen.

1. Introduction

Manganese is one of the most abundant first-row transition elements in nature [1] and plays a significant role in biological systems. For example, manganese-based active sites can be found in superoxide dismutase [2], Mn-catalase [2] and the oxygen-evolving complex of Photosystem II [3]. The manganese cores are critical for the activity of these enzymes and take part in important proton-coupled electron-transfer (PCET) reactions [4]. Moreover, manganese-based molecular catalysts have attracted a lot of the scientific interest, since manganese can cycle through the oxidation states of II, III, IV, VII and even the less stable V and VI oxidation states. Many manganese-based catalysts have been developed for challenging chemical reactions like the photocatalytic reduction of CO_2 to CO [5], dioxygen activation [6] and various organic oxidative transformations [7]. It has been proven that the coordination of deprotonated amides helps the isolation of manganese complexes in these important higher oxidation states by providing stability to the metal center through their negative charge [8]. By using deprotonated amido-ligands, complexes of Mn(III) [9], Mn(IV) [10] and Mn(V) [11] have been successfully isolated and structurally characterized.

Tripodal ligands have found application in various scientific fields including biomimetic synthesis [12], small molecule catalysis [13], synthesis of sensors [14] and synthesis of NO releasing molecules to treat cancer [15,16]. In the field of catalysis, tripodal ligands, are frequently used due to their ability to occupy most of the coordination sites around the metal leaving only one axial position available for the substrate (Scheme 1). This is inspired by the way enzymes work in nature, where they achieve extraordinary reactivity and selectivity by creating a substrate-specific active site for the coordination and activation of the substrate [17].

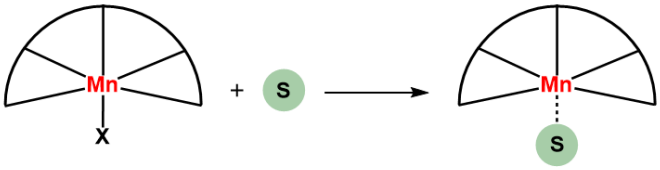

Scheme 1. Schematic representation of the coordination of the substrate to the ‘’active site’’ of the Mn(II) complexes.

More specifically, water oxidation catalysis has attracted a lot of the scientific interest in the recent years. Water oxidation plays a crucial role in both natural and artificial photosynthesis [18], which is an attractive solution to the depletion of fossil fuels as energy sources due to the increasing consumption. Through artificial photosynthesis the sun’s light energy can be converted and stored in chemical bonds and can be used as fuel (hydrogen generation from water splitting eq. 1-3) [19]. However, the efficiency of artificial photosynthesis, is greatly hindered by the slow kinetics of the water oxidation reaction. The most efficient water oxidation catalyst in nature is the oxygen-evolving complex (OEC) in photosystem II, which contains a multinuclear manganese core ($CaMn_4O_5$) and can achieve a turnover frequency (TOF) of 400 s^{-1} [20]. Inspired by this system, many multinuclear manganese complexes have been developed as catalysts for water oxidation and many of them showed efficient results, such as $[OH_2(terpy)Mn(O)_2Mn(terpy)OH_2]$ [21a], $[Mn_4O_4L_6]$ [21b], $[Mn_4V_4O_{17}(OAc)_3]$ [21c] and the newly reported Mn_{12} clusters bearing -OH groups [21d]. The high efficiency of these complexes is attributed to the multinuclear sites which are believed to play a significant role to the O-O formation of the water oxidation reaction [22]. However some mononuclear manganese complexes (for example $[(Py_2N(t\text{Bu})_2)Mn(H_2O)_2]$ [21e]) have also showed promising results for water oxidation.

$$2H_2O\ (l) \rightarrow 4H^+\ (aq) + O_2\ (g) + 4e^- \quad (1)$$

$$4H^+\ (aq) + 4e^- \rightarrow 2H_2\ (g) \quad (2)$$

$$2H_2O\ (l) \rightarrow 2H_2\ (g) + O_2\ (g) \quad (3)$$

Herein, it is reported the synthesis, structural and physicochemical characterization of three manganese(II) complexes of the general formula $[Mn^{II}(trip)X]$ (X = Cl^-, Br^-, I^-) with the novel, tripodal-amidate ligand *N*-{2-[(bis(pyridine-2-ylmethyl)amino)methyl]phenyl}picolinamide (Htrip) (Scheme 2). Moreover, the potential application of these manganese(II) complexes as water oxidation catalysts is also reported.

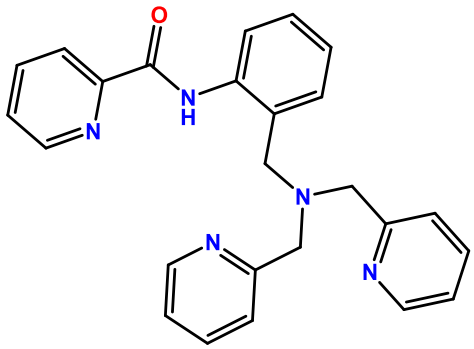

Scheme 2. The tripodal ligand (Htrip) used in this study.

2. Experimental

2.1. Materials, General Methods

All chemicals and solvents were purchased from Sigma-Aldrich and Merck, were of reagent grade, and were used without further purification. C, H, and N analyses were conducted by the microanalytical service of the School of Chemistry, the University of Glasgow. FT-IR transmission spectra of the compounds, in KBr pellets, were acquired using a JASCO Model 460 spectrophotometer in the 4000−400 cm^{-1} range. Ethyl alcohol was dried over magnesium(II) ethoxide and distilled just prior to its use. Merck silica gel 60 F254 TLC plates

were used for thin layer chromatography. The UV-Vis spectra were performed in a SHIMADZU UV-Vis 2600.

2.2. Preparations

2.2.1. Synthesis of N-(2-((bis(pyridine-2-ylmethyl)amino)methyl)phenyl)picolinamide, (Htrip) (Scheme 3). 2-Nitrobenzaldehyde (1.00g, 6.6 mmol) was added to a stirred solution of bis(2-pyridylmethyl)amine (1.31g, 6.6 mmol) in dry CH_2Cl_2 (20 ml). After 30 min of stirring at room temperature (20 ^{0}C), sodium triacetoxyborohydride (2.23g, 10.5mmol) was added and the resulting mixture was stirred overnight at room temperature (20 ^{0}C). 5% aqueous $NaHCO_3$ (20 mL) was then added, and the mixture was extracted with CH_2Cl_2 (2 x 15 mL). The organic layer was separated, dried over magnesium sulfate and the solvent was removed under vacuum. The resulting product was purified by column chromatography and was dissolved in 50 mL of MeOH. 0.35g of hydrogenation catalyst (10% Pd on activated carbon) was added to this solution and pure hydrogen was admitted for 24h under magnetic stirring. The mixture was filtered, and the filtrate was evaporated to dryness to yield a yellow oil. The oil was dissolved in dry THF and pyridine-2-carbonyl chloride hydrochloride (1.25 g, 7 mmol) and triethylamine (2.1 ml, 15 mmol) were added to it. The mixture was stirred overnight at room temperature (20 ^{0}C) and the solvent was removed under vacuum. 5% aqueous $NaHCO_3$ (20 mL) was added to the solid, and the mixture was extracted with CH_2Cl_2 (2 x 15 mL). The organic layer was separated, dried over magnesium sulfate and the solvent was removed under vacuum to give a light-yellow oil. The product was purified by recrystallisation from diethyl ether to give the final product as a white powder. Yield (1.16g, 43% based on 2-nitrobenzaldehyde). Anal. calcd for $C_{25}H_{23}N_5O$: C, 73.33; H, 5.66; N, 17.10. Found: C, 73.26; H, 5.74; N, 17.04. ESI(+) HRMS: calcd for $[M+H]^+$: *m*/*z* 410.1975. Found: 410.1958 (100%). ^{1}H and ^{13}C NMR and UV-vis spectra of the organic molecule Htrip are shown in Figures S5, S6, and S7 respectively.

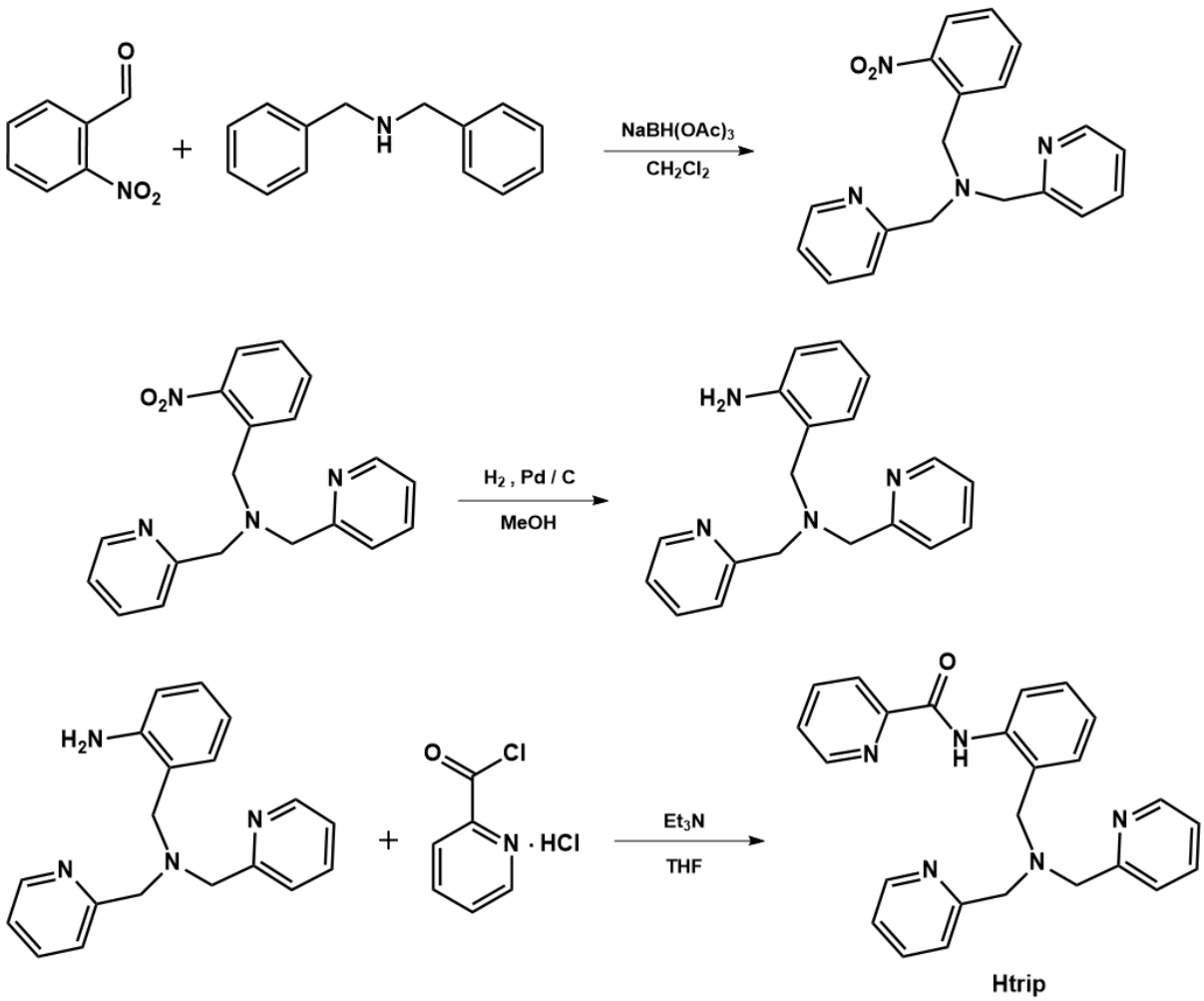

Scheme 3. Synthesis of the ligand Htrip.

2.2.2. Synthesis of (Chlorido) {N-{2-[(bis(pyridine-2-ylmethyl)amino)methyl]phenyl}picolinamido-N_{py},N_{py},N_{am},N_{ami},N_{pic}}manganese(II), [Mn^{II}(trip)Cl] ***(1).*** $MnCl_2 \cdot 4H_2O$ (73 mg, 0.37 mmol) was dissolved in dry ethyl alcohol (10 ml) under high purity argon and magnetic stirring. Solid Htrip (150 mg, 0.37 mmol) was added to the stirred solution in one portion and its color turned to light yellow. Then, sodium ethoxide (30 mg, 0.44 mmol) was added to it and its color changed to orange and a small amount of white precipitate (NaCl) was formed. The mixture was stirred at room temperature overnight, the solvent was evaporated to dryness under vacuum, and the residue was extracted with $CHCl_3$ (25 ml) and filtered to remove insoluble salts. The volume of the filtrate was reduced to 5 ml under vacuum and diethyl ether (30 ml) was added dropwise under constant stirring to get

0.135 g of a yellow solid. Yield: (73%, based on Htrip). Anal. calcd for ($C_{25}H_{22}ClN_5OMn$ M_r = 498.87): C, 60.19; H, 4.45; N, 14.04. Found: C, 60.23; H, 4.59; N, 13.94. μ_{eff} = 5.81 BM.

Crystals of **1** suitable for X-ray diffraction analysis were obtained by layering diethyl ether into a concentrated dichloromethane solution of **1.**

2.2.3. Synthesis (Bromido) {N-{2-[(bis(pyridine-2-ylmethyl)amino)methyl]phenyl}picolinamido-N_{py},N_{py},N_{am},N_{ami},N_{pic}}manganese(II), [Mn^{II}(trip)Br] ***(2).*** The compound **2** was prepared (in 69% yield, based on Htrip) in the same way as compound **1** except that $MnBr_2 \cdot 4H_2O$ (105 mg, 0.37 mmol) was used instead of $MnCl_2 \cdot 4H_2O$. The colour of the compound **2** was also yellow. Anal. calcd for $C_{25}H_{22}BrN_5OMn$ (M_r = 543.33): C, 55.27; H, 4.08; N, 12.89. Found: C, 55.33; H, 4.09; N, 12.81. μ_{eff} = 5.97 BM.

Crystals of **2** suitable for X-ray diffraction analysis were obtained by layering diethyl ether into a concentrated dichloromethane solution of **2**.

2.2.4. Synthesis of (Iodido) {N-{2-[(bis(pyridine-2-ylmethyl)amino)methyl]phenyl}picolinamido-N_{py},N_{py},N_{am},N_{ami},N_{pic}}manganese(II), [Mn^{II}(trip)I] ***(3).*** MnI_2 (113 mg, 0.37 mmol) was dissolved in dry ethyl alcohol (10 ml) under high purity argon and magnetic stirring. Solid Htrip (150 mg, 0.37 mmol) was added to the stirred solution in one portion and its color turned to orange yellow and then, sodium ethoxide (30 mg, 0.44 mmol) was added to it and the color of the solution changed to light yellow. The mixture was stirred at room temperature overnight, filtered and layered with diethyl ether to obtain X-ray quality, 0.042 g of orange crystals of **3**. Yield: (19%, based on Htrip). Anal. calcd for $C_{25}H_{22}IN_5OMn$ (M_r = 590.33): C, 50.87; H, 3.76; N, 11.86. Found: C, 50.79; H, 3.84; N, 11.94. μ_{eff} = 5.79 BM.

2.3. Crystal data collection and refinement

Suitable crystals were glued to a thin glass fibber with cyanoacrylate (super glue) adhesive and placed on the goniometer head. Diffraction data were collected on a Bruker D8 Quest Eco diffractometer, equipped with a Photon II detector and a TRIUMPH (curved graphite) monochromator utilizing Mo Ka radiation ($\lambda = 0.71073$ Å) using the APEX 3 software package [23]. The collected frames were integrated with the Bruker SAINT software using a narrow-frame algorithm. Data were corrected for absorption effects using the Multi-Scan method (SADABS) [24]. The structures were solved using the Bruker SHELXT Software Package and refined by full-matrix least squares techniques on F2 (SHELXL 2018/3) [25] via the ShelXle interface [26]. The non-H atoms were treated anisotropically, whereas the organic H atoms were placed in calculated, ideal positions and refined as riding on their respective carbon atoms. All compounds were refined as inversion twins; Flack parameters, x, are included in Table 1. PLATON [27] was used for geometric calculations, and Diamond [28] for molecular graphics.

Details on data collection and refinement are presented in Table 1. Full details on the structures can be found in the CIF files in the ESI. CCDC 2067257-2067259 contain the supplementary crystallographic data for this paper. These data can be obtained free of charge via www.ccdc.cam.ac.uk/data_request/cif.

Table 1 Crystal data and details of the structure determination and refinement for the manganese(II) compounds **1**, **2**, and **3**.

Compound	**1**	**2**	**3**
Empirical formula	$C_{25}H_{22}ClMnN_5O$	$C_{25}H_{22}BrMnN_5O$	$C_{25}H_{22}IMnN_5O$
Formula weight	498.86	543.32	590.31
Crystal system	monoclinic	monoclinic	monoclinic
Space group	$P2_1$	$P2_1$	$P2_1$
Unit cell dimensions *a*, *b*, *c* (Å), *β* (°)	8.6669(7), 15.6858(13), 9.2712(7), 113.570(3)	8.6950(4), 15.6878(7), 9.2885(4), 113.388(2)	8.7948(3), 15.7519(6), 9.3991(4), 112.746(1)
Volume ($Å^3$)	1155.24(16)	1162.90(9)	1200.84(8)
Density (calculated) (g/cm^3)	1.434	1.552	1.633
Absorption coefficient (mm^{-1})	0.715	2.313	1.862
F(000)	514	550	586
θ range for data collection	2.721 to 26.369°	2.552 to 26.993°	2.586 to 24.999°
Reflections collected	15867	41346	24729
Independent reflections	4720 [R_{int} = 0.0824]	5059 [R_{int} = 0.1076]	4212 [R_{int} = 0.0308]
Data / restraints / parameters	4720 / 1 / 299	5059 / 1 / 299	4212 / 1 / 298
Flack parameter, *x*	0.44(5)	0.23(2)	-
Goodness-of-fit	1.076	1.051	1.114
Final R indices [I > 2σ(I)]	R_{obs} = 0.0748, wR_{obs} = 0.1422	R_{obs} = 0.0602, wR_{obs} = 0.1775	R_{obs} = 0.0145, wR_{obs} = 0.0384
R indices [all data]	R_{all} = 0.1047, wR_{all} = 0.1528	R_{all} = 0.0691, wR_{all} = 0.1835	R_{all} = 0.0152, wR_{all} = 0.0384
Largest diff. peak and hole (e/ $Å^3$)	0.675 and -0.732	1.321 and -1.286	0.254 and -0.378

R = Σ||Fo|-|Fc|| / Σ|Fo|, wR = {Σ[w(|Fo|2 - |Fc|2)2] / Σ[w(|Fo|4)]}1/2 and w=1/[σ2(Fo2)+(aP)2+bP] where P=(Fo2+2Fc2)/3. 1: a = 0.0668, b = 0.1209; 2: a = 0.1305, b = 0.9700; 3: a = 0.0200, b = 0.0844.

2.4. Electrochemistry

Electrochemical measurements were performed under an argon atmosphere, at room temperature, in either dichloromethane or dimethylformamide (DMF) solutions containing 0.1 M Et_4NBF_4 as a supporting electrolyte, and 1 mM of the manganese complex or the ligand Htrip in a CHI650E potentiostat equipped with a three-electrode cell. The scan rate was 100 mV s^{-1} unless otherwise stated. The working electrode was a glassy carbon disk, and a platinum wire was used as a counter electrode. The potential was measured against a $Ag/AgNO_3$ reference and converted to the normal hydrogen electrode (NHE) potential by recording the CVs of DMF or CH_2Cl_2 solutions of ferrocene (0.65 V *vs* NHE). The potential values are reported against NHE throughout the manuscript. Exhaustive electrolysis was performed in CH_2Cl_2 solution using platinum mesh as a working electrode, a $Ag/AgNO_3$ as a reference electrode and a platinum wire separated with a Teflon frit from the solution as auxiliary electrode. But_4NBF_4 0.2 M was used as electrolyte. The solvents CH_2Cl_2 and DMF were dried over CaH_2 and distilled just prior to their use. DMF was distilled under reduced pressure. The simulation of CVs was performed using the program CVSim.

3. Results and discussion

3.1. Description of the structures

Interatomic distances and bond angles relevant to the manganese(II) coordination sphere are listed in Table 2. The molecular structure of compound **1** is presented in Fig. 1, and the structures of **2** and **3** in Fig. 2. Compounds **1** – **3** crystallize in the monoclinic space group $P2_1$. The origin of the chirality of the compounds is located on the 2-methylenephenyl moiety which connects the amino and the amido parts of the ligand, and upon coordination can be turned to different sites. That can be easily seen in Fig. 2, comparing the position of the linker in the structures of compounds **2** and **3**. They are isostructural with minor differences induced by the presence of a different halogen in each compound. It is noteworthy that the lattice dimensions

and consequently the volume of the unit cell, though very similar, appear to increase systematically with the size of halogens from Cl^- in **1** to I^- in **3**. Due to the similarity of the structures, only the structure of **1** will be described in detail.

The manganese(II) atom in **1** occupies the center of a distorted octahedral coordination sphere consisting of two pyridine, one picoline and one amino nitrogen atoms on the equatorial plane while the axial positions are occupied by one amido nitrogen atom and the halogen anion.

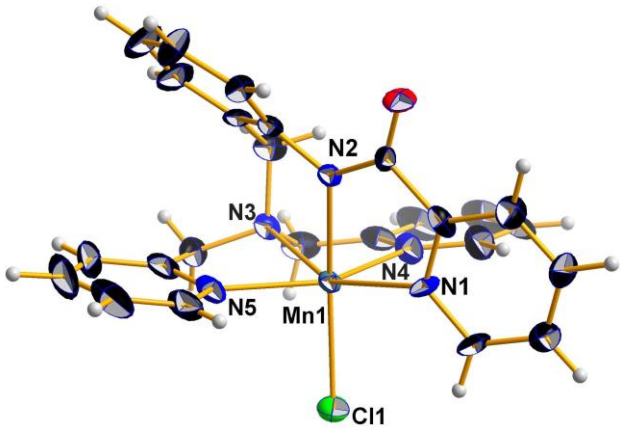

Fig. 1 A thermal ellipsoid plot (50% probability level) of the molecular structure of **1** with a partial labeling scheme.

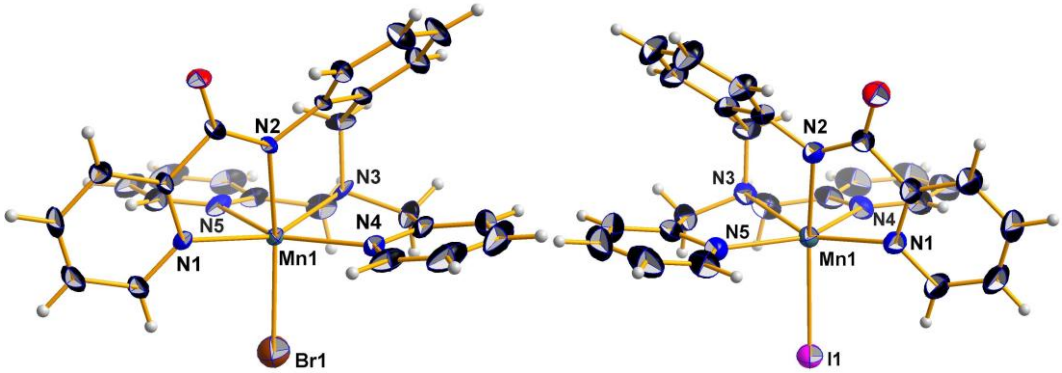

Fig. 2. Thermal ellipsoid plots (50% probability level) of the molecular structures of **2** and **3.**

Compound **1** belongs to a small group of manganese(II) complexes coordinated to tripodal-amidate ligands, which contain five nitrogen donor atoms: one amino, one amido, and three heterocyclic nitrogen atoms [29]. There are only a few similar Mn(II) complexes and these can

be separated in two distinct groups; a) there are six complexes where the sixth donor atom comes from a coordinated NO and leads to low spin diamagnetic species [30-32]. These complexes are considered rather as $\{Mn^{I}(N5_{trip})NO\}^{+}$ species. and b) there is only one compound where the sixth coordination position of the octahedron is a conventional donor, specifically an oxygen atom belonging to the N-coordinated amido moiety of an adjacent complex [33]. The complexes presented in this study belong to the second group, and their structural characteristics can only be compared to those of 1D-polymer-$[Mn^{II}(dpaq^{2Me})](OTf)$ (where $dpaq^{2Me}$ is 2-[bis(pyridin-2-ylmethyl)]amino-N-2-methyl-quinolin-8-yl-acetamidate and OTf is the trifluoromethanesulfonate anion) [33] (Scheme 4). Thus, the three manganese(II) complexes **1**-**3** constitute the first examples of mononuclear $\{Mn^{II}(N5_{trip})X\}$ species to be reported.

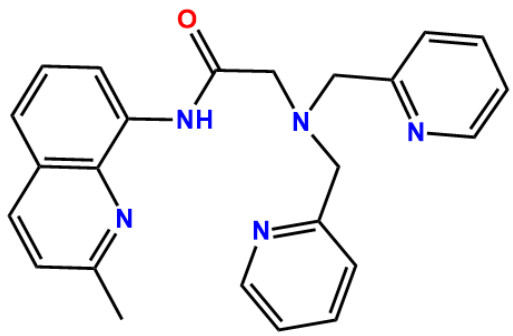

Scheme 4. The ligand $Hdpaq^{2Me}$.

In **1**, the Mn^{II}-N bond distances span the range 2.205 – 2.325 Å, and they are in good agreement with the literature data. The shortest distance belongs to the $Mn^{II} – N_{amido}$ bond, which becomes even shorter as the coordinated halogen in trans position changes from Cl^{-} to Br^{-} to I^{-}. So, the corresponding $Mn^{II} – N_{amido}$ and $Mn^{II} – X$ pairs of distances are: 2.205(8) and 2.436(3) Å for **1**, 2.199(7) and 2.552(2) for **2**, and 2.192(3) and 2.838(1) for **3**, concurring with the trans influence of the halides.

The deviation of **1** from the ideal octahedral geometry, apart from the bond distances, can easily be seen from both the cis and trans angles of the coordination sphere which span the ranges 72.37 – 124.32 and 146.30 – 165.30 ^{o} respectively. These distortions appear to be larger than literature's example [33], and we believe that this is due to the presence of a 6-membered chelate ring (instead of a 5-membered one) in the coordination sphere of Mn^{II} in **1**, with respect to the change of the "hinge" connecting the amino with the amido nitrogen atoms (a 2-methylenephenyl group in our case, a methylenecarbonyl group in the case of $[Mn^{II}(dpaq^{2Me})]^{+}$). Additionally, there is an intramolecular $\pi - \pi$ interaction between the phenyl ring and one of the pyridine rings (centroid distance: 3.8 Å, angle between least square planes: 34.55 ^{o}, distance of one ring's centroid to the least square plane of the other ring: 3.6 Å) which eventually hauls the picolinamide moiety, leading to two very different $N_{picoline} - Mn^{II} - N_{pyridine}$ angles. (88.13 and 124.32^{o} compared to the corresponding 102.85 and 107.03^{o} literature values) [33].

To quantify the distortions from the ideal octahedral geometry the program OctaDist [34] was utilized, which calculates the parameters ζ, Σ and Θ. ζ is the average of the sum of the deviation of six unique Mn–donor atom bond lengths from the average value; Σ is the sum of the deviation of 12 unique *cis* donor atom–metal–donor atom angles from 90 °; and Θ is defined as the degree of trigonal distortion of the coordination geometry from an octahedron towards a trigonal prism, it is the sum of the deviation of 24 unique torsional angles between the ligand atoms on opposite triangular faces of the octahedron viewed along the pseudo-threefold axis from 60 °. In an ideal octahedron all those parameters should be equal to zero. In our case their values are: ζ = 0.354 Å, Σ = 125.8 ^{o} and Θ = 482.7 ^{o} showing a severe distortion from the ideal polyhedron.

Table 2 Interatomic distances (Å) and angles (°) relevant to the manganese(II) coordination sphere for the manganese(II) compounds **1**, **2** and **3**.

Parameter	**1**	**2**	**3**
Mn(1) - X[a]	2.436(3)	2.551(2)	2.8404(7)
Mn(1) – N(1)	2.231(9)	2.238(8)	2.236(3)
Mn(1) – N(2)	2.205(9)	2.199(7)	2.193(3)
Mn(1) – N(3)	2.294(8)	2.298(7)	2.290(3)
Mn(1) – N(4)	2.325(6)	2.269(7)	2.323(2)
Mn(1) – N(5)	2.265(8)	2.325(5)	2.278(3)
X – Mn(1) – N(1)	96.2(2)	95.4(2)	95.52(8)
X – Mn(1) – N(2)	165.3(2)	165.2(2)	165.53(7)
X – Mn(1) – N(3)	104.9(2)	104.3(2)	102.75(7)
X – Mn(1) – N(4)	93.1(2)	92.4(2)	91.60(7)
X – Mn(1) – N(5)	93.1(2)	93.0(2)	90.89(7)
N(1) – Mn(1) – N(2)	73.6(3)	74.1(3)	74.8(1)
N(1) – Mn(1) – N(3)	151.7(3)	152.8(3)	154.1(1)
N(1) – Mn(1) – N(4)	88.1(3)	124.5(3)	89.1(1)
N(1) – Mn(1) – N(5)	124.3(3)	88.2(3)	124.0(1)
N(2) – Mn(1) – N(3)	88.4(3)	89.2(3)	90.03(9)
N(2) – Mn(1) – N(4)	97.1(3)	85.5(3)	98.8(1)
N(2) – Mn(1) – N(5)	85.3(3)	96.8(3)	85.91(9)
N(3) – Mn(1) – N(4)	72.4(3)	73.9(3)	72.42(9)
N(3) – Mn(1) – N(5)	74.1(3)	72.4(3)	74.32(9)
N(4) – Mn(1) – N(5)	146.3(3)	146.2(3)	146.4(1)

[a] X corresponds to Cl(1), Br(1) and I(1) for compounds **1**, **2** and **3** respectively.

3.2 Infrared Spectra

Table 3 depicts the assignments of some diagnostic bands for the ligand Htrip and its manganese(II) complexes. Complexes **1-3** have almost the same infrared bands and therefore only complex **1** will be discussed. The medium-intensity band at 3332 cm^{-1} in the spectra of

the ligand was assigned to the $(N\text{-}H)_{amide}$ stretching vibration, $\nu(NH)$. Due to the amide deprotonation of the ligand in complex **1**, the $\nu(NH)_{amide}$ band is absent from the spectra of the complex as expected. The bands at 1533 cm^{-1} and 1291 cm^{-1} in the spectrum of the free ligand were assigned to the amide II and amide III bands respectively and are caused by the coupling of the $\nu(CN)_{amide}$ and $\delta(NH)_{amide}$ modes. In the spectra of the complexes the amide II and amide III bands are replaced by a strong band at 1367 cm^{-1}. This replacement might be expected as the removal of the amide proton produces a pure C-N stretch [35]. The ν(C=O) band (amide I) appears as a strong band at 1670 cm^{-1} in the spectra of Htrip (Fig. 3). This band appears at lower wavenumbers in the spectra of the complexes (1605 cm^{-1}) (Fig. 3). This shift to lower wavenumbers for the ν(C=O), is expected because the amide deprotonation and the *N*-coordination to the metal cause a decrease of the carbonyl double bond character.

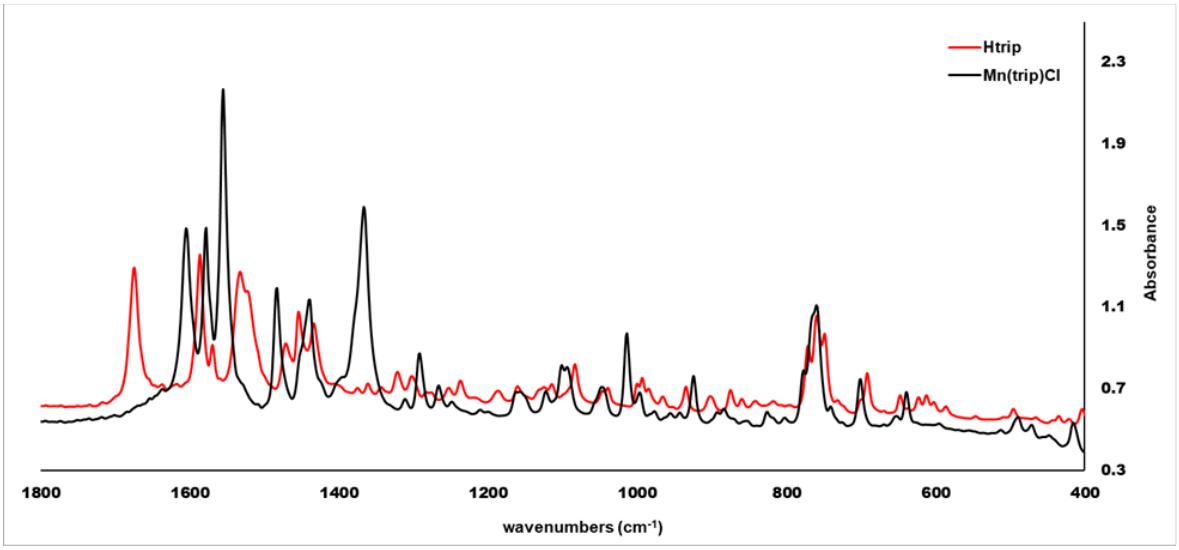

Fig. 3. Comparison of the IR spectra of the ligand and compound **1**.

Table 3 Diagnostic infrared bands [cm-1] of the ligand Htrip and its manganese(II) compounds.

	ν(NH)	*ν*(CO)[a]	amide II[b]	*ν*(CN)$_{amide}$	amide III[b]
Htrip	3332	1670	1533	-	1291
1	-	1605	-	1367	-
2	-	1605	-	1366	-
3	-	1603	-	1368	-

[a]In secondary amides the *ν*(C=O) vibration is called amide I. [b]In secondary amides, these bands arise from coupled *ν*(CN) and *δ*(NH) modes.

3.3 Electrochemistry

The cyclic voltammograms (CVs) for the ligand Htrip and the manganese(II) compounds **1** and **2** are illustrated in Fig. 4, 5 and 6 respectively. The CV for the ligand Htrip revealed two strong multielectron irreversible redox peaks at 1.157 and 1.318 V (Fig. 4). The CV for compound **1** in CH_2Cl_2 (Fig. 5) shows a well-defined redox couple at 0.645 V (ΔE = 76 mV), in addition to the two irreversible ligand centered redox peaks (not shown in Fig. 5). Thus, the redox process at 0.645 V was assigned to the oxidation of manganese(II). The CV for compound **1** in DMF (Fig. 5) also shows a redox couple at 0.598 V (ΔE = 73 mV), in addition to the two irreversible ligand centered redox peaks (not shown in Fig. 5). The CV for compound **2** (Fig. 6) revealed a very similar behavior with **1** in both solvents and thus, it will not be further discussed. The CV for compound **3** in DMF (in CH_2Cl_2 this compound is not soluble) is shown in Fig. S1. Compound **3** also showed a redox couple at 0.613 V assigned to the oxidation of manganese(II).

The number of electrons of the metal centered redox processes at ~0.60 V was measured by exhaustive electrolysis of the manganese(II) complexes at 0.70 V. The number of electrons at

95% of the initial electrolysis current was 1.85. The CVs of the CH_2Cl_2 solution of **2** after electrolysis remain the same and this presumably mean that that this redox process is fully reversible (Fig. 7). The brown color of the CH_2Cl_2 solution of **2** after electrolysis changed to green and its UV-Vis spectrum (Fig. 8) exhibits two peaks at 727 (ε = 610 M^{-1} cm^{-1}) and 374 nm (ε = 1181 M^{-1} cm^{-1}) and is like the spectrum of [Mn^{IV}Clsalen] [36]. Apparently, the metal centred reversible redox processes of complexes **1** – **3** are of $2e^-$ and were assigned to Mn^{II}-Mn^{IV} redox couple. At this point, it is worth noting that mononuclear or multinuclear manganese(IV) compounds are stabilized by either ligands containing nitrogen donor atoms [37-40] or ligands with mixed nitrogen and oxygen donor atoms [41]. Based on Hard-Soft Acid-Base (HSAB) theory someone expects harder donor atoms such as oxygen donor atoms to stabilize better Mn^{IV}, which is a hard acid, than nitrogen donor atoms. On the other hand, the splitting of the *d* orbitals by the nitrogen donor atoms is larger than oxygen donor atoms, and thus, nitrogen atoms can stabilize Mn^{IV} by crystal field stabilization energy (CFSE). This stabilization is expected to be significant for metal ions having d^3 electronic configuration such as Mn^{IV}. Therefore, it is crystal clear that the stabilization of Mn^{IV} by coordination of the ligand $trip^-$ might be a result of the ligation of the nitrogen atoms to Mn^{IV}, through CFSE, and the strong coordination of the deprotonated amide nitrogen which satisfies the electron needs of Mn^{IV}.

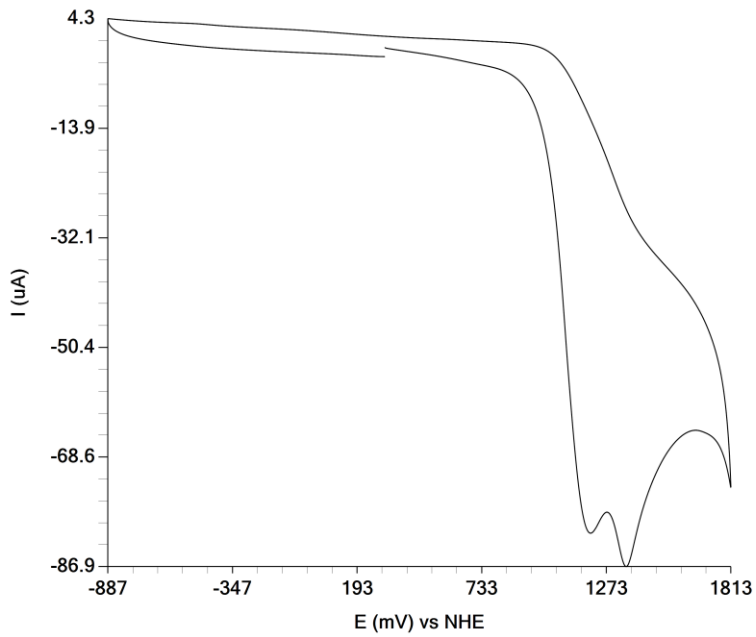

Fig. 4. Cyclic voltammogram of the ligand Htrip in DMF solution.

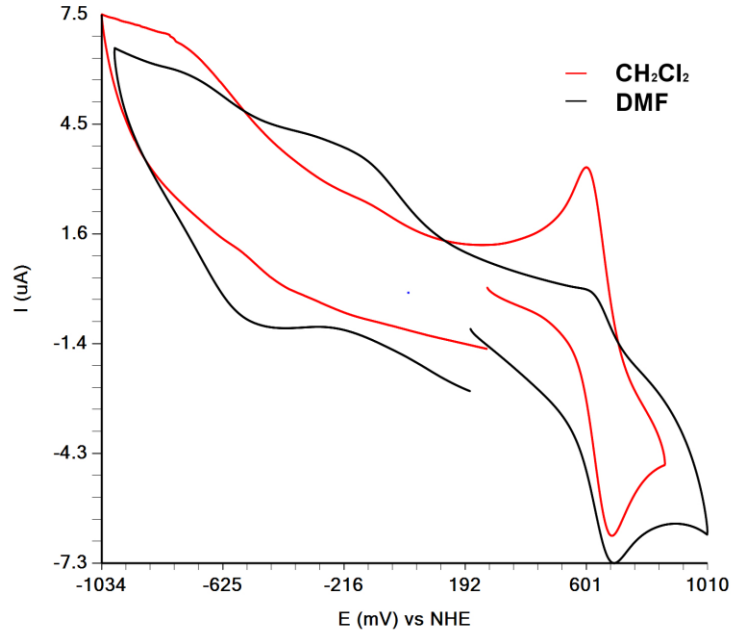

Fig. 5. Cyclic voltammograms of the manganese(II) complex **1** in CH_2Cl_2 and in DMF solutions.

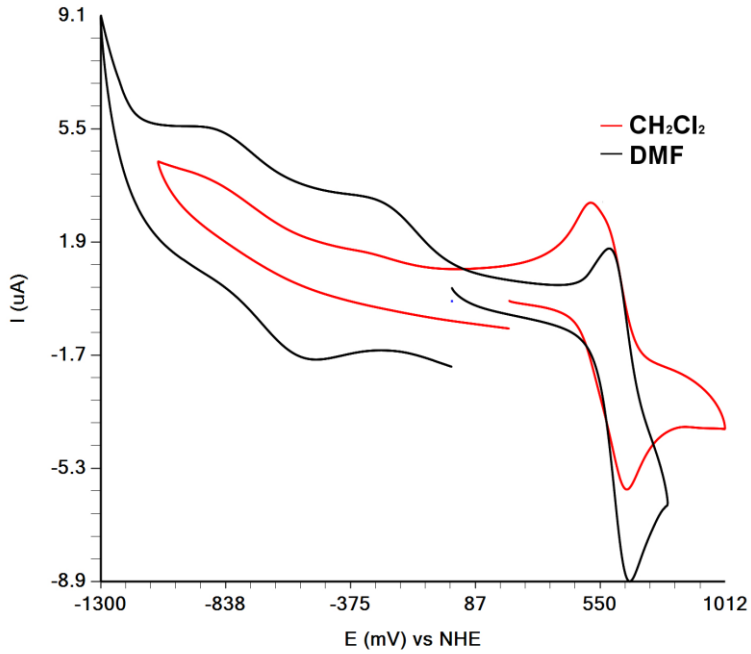

Fig. 6. Cyclic voltammograms of the manganese(II) complex **2** in CH_2Cl_2 and in DMF solutions.

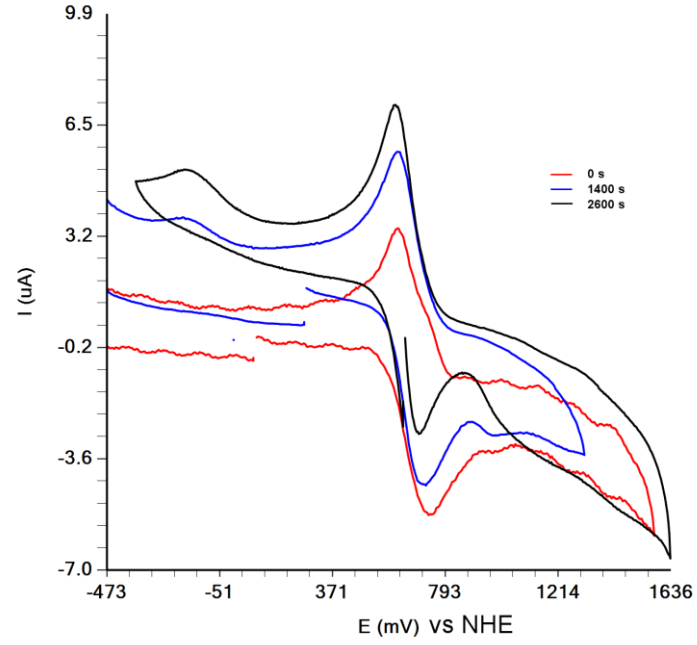

Fig. 7. CVs of a CH_2Cl_2 solution (1 mM) of **2** at time 0, 1400 and 2600 s (0%, 65% and 87% of the initial current respectively) after the commencement of the exhaustive electrolysis at 0.70 V.

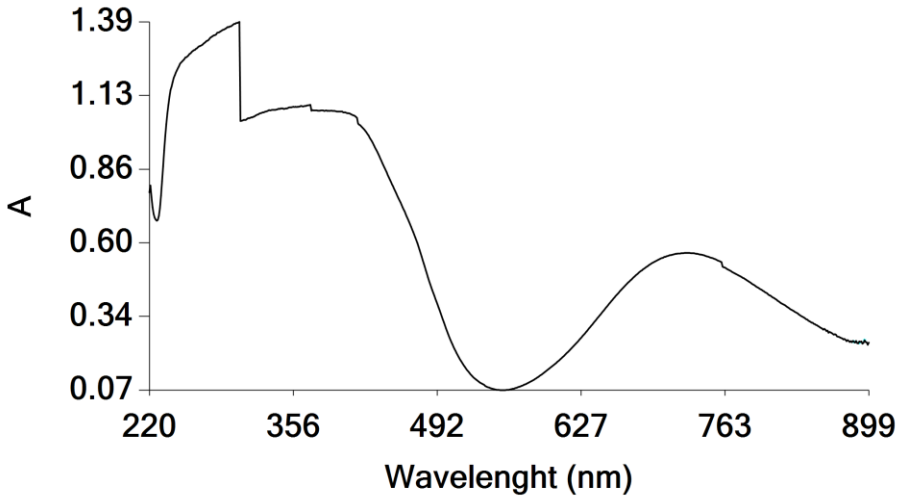

Fig. 8. UV-Vis of a CH_2Cl_2 solution (1 mM) of **2** after the end of exhaustive electrolysis at 0.70 V.

*3.4 Water Oxidation by the ligand Htrip, **1** and **2***

The electrochemical properties for oxygen evolution reaction (OER) of the ligand Htrip have been investigated in a DMF solution containing 1.0 mM Htrip (Fig. 9). Upon gradual addition of water to a DMF solution of ligand Htrip, the CVs show a decrease of the anodic current of the ligand's oxidation peaks (Fig. 9). This decrease might be attributed to either the interaction of the ligand with water, i.e., hydrogen bonding, or to an associated chemical reaction or both. A cathodic peak at -0.50 V (Fig. 9) associated with the oxidation peaks of the ligand (Fig. S2), which appears upon addition of water to the DMF solution, was assigned to the reduction of dioxygen to H_2O. The current of this cathodic peak is increasing by increasing the quantity of water to the DMF solution (Fig. 9). The origin of the cathodic peak was confirmed by spike experiments, after addition to the DMF solution of either O_2 or H_2O_2.

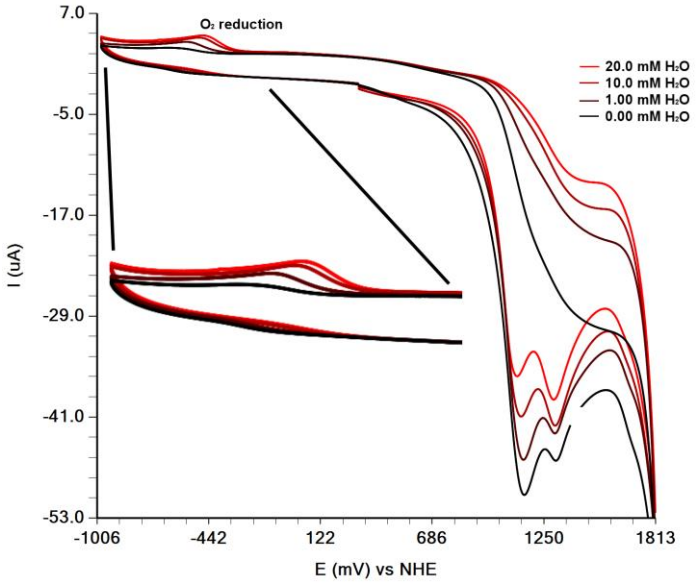

Fig. 9. CVs of the ligand Htrip in DMF solution upon gradual addition of H_2O.

The electrochemical properties for OER of the manganese(II) complex **1** have been also investigated in DMF solution containing **1** (1.0 mM, Fig. 10). Upon gradual addition of water to a DMF solution of **1**, the CVs also show a decrease of the anodic current of the ligand's oxidation peaks at 1.155 and 1.326 V (Fig. 10). The current decrease of these two peaks in **1** upon gradual addition of water to DMF solution is larger than the corresponding decrease of ligand's oxidation peaks with the same concentration of water (Fig. 9). Moreover, upon the gradual addition of water to the DMF solution a negative shift of the ligand's oxidation peak at 1.155 V and a positive shift of the ligand's oxidation peak at 1.326 V occurs. When the concentration of water to the DMF solution becomes higher than 10 mM, the ligand's oxidation peaks diminish dramatically. At this point, it is worth noting that the wave at 0.60 V, due to manganese oxidation, remains intact during all the electrochemical measurements and thus, it is reasonable to assume that **1** retains its integrity.

At voltage higher than 1.369 V the current (Fig. 10) is increasing upon gradual addition of water and this increase was assigned to the catalytic oxidation of water to dioxygen. This assignment was supported by the normalized catalytic currents ($i_{cat}/u^{1/2}$, u = scan rate), which they decreased by increasing the scan rates (Fig. 11).

The two anodic peaks which correspond to the oxidation of the ligand are associated with the cathodic peak at -0.50 V assigned to the reduction of O_2 to H_2O. This is supported from the CVs at various switching potentials, showing that the cathodic peak at -0.5V emerges in the switching potentials ranging from 1.2 to 1.8 V (Fig. 12). Thus, the experiment supports that the oxidized species of the ligand react and oxidize H_2O. Photoinduced or electro-catalysed oxidation of water from organic molecules or ligands in metal organic complexes have been reported previously [42,43]. A common element in these molecules is the presence of delocalized π-systems. Thus, the electrocatalytic oxidation of water from trip$^-$ in **1-3** might be attributed to the presence of the extended π-systems of the organic ligand.

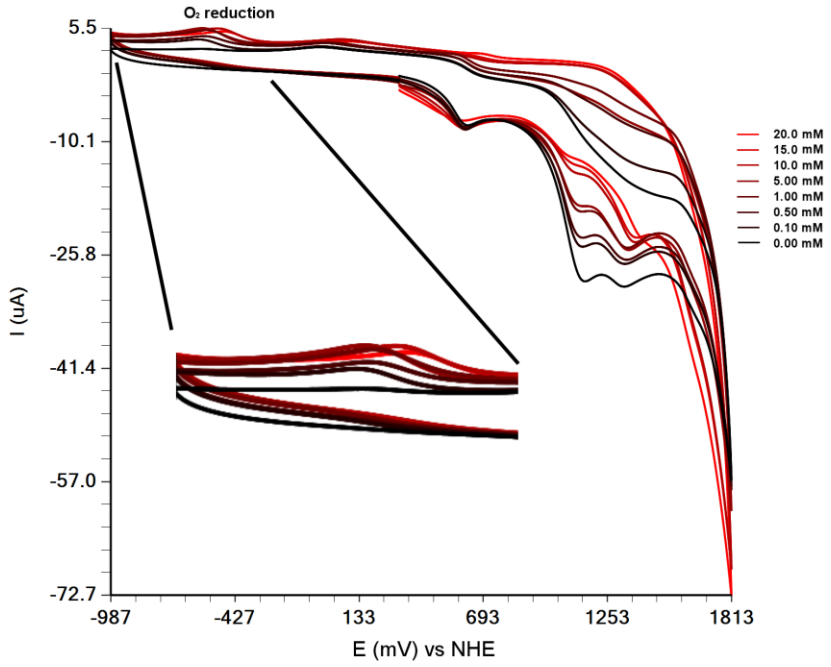

Fig. 10. CVs of the manganese(II) complex **1** in DMF solution upon gradual addition of H_2O. Scan rate 25 mV s^{-1}.

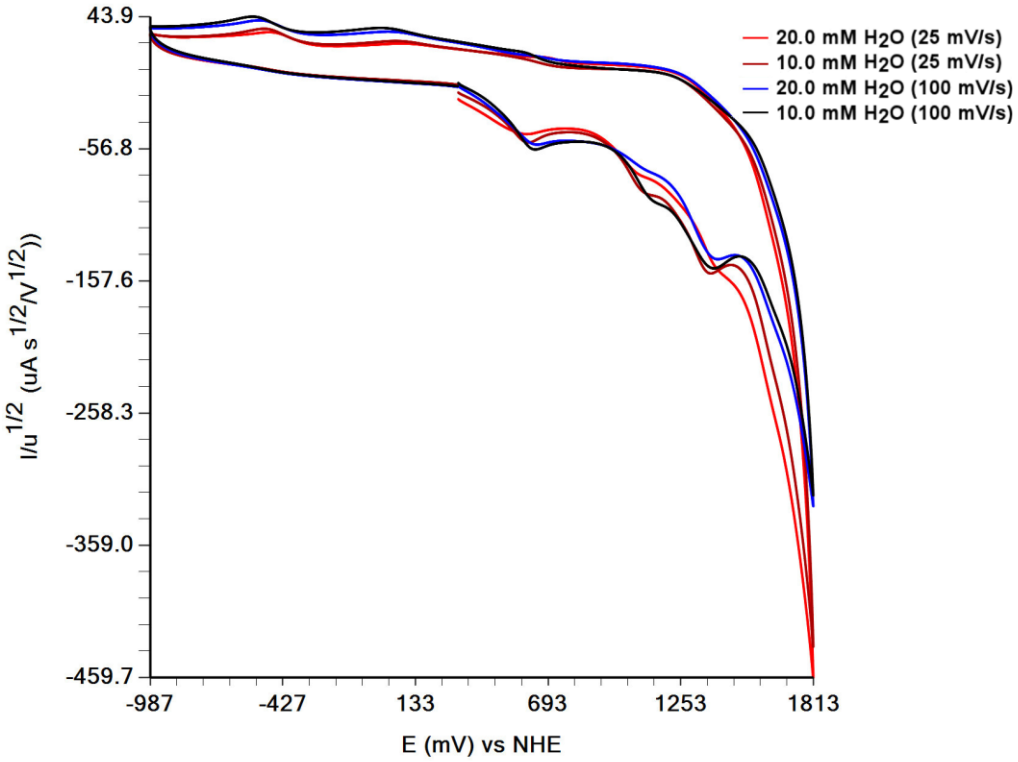

Fig. 11. Normalized CVs of the manganese(II) complex **1** in DMF containing water (10.0 and 20.0 mM) at two scan rates 25 and 100 mV/s for both concentrations of water.

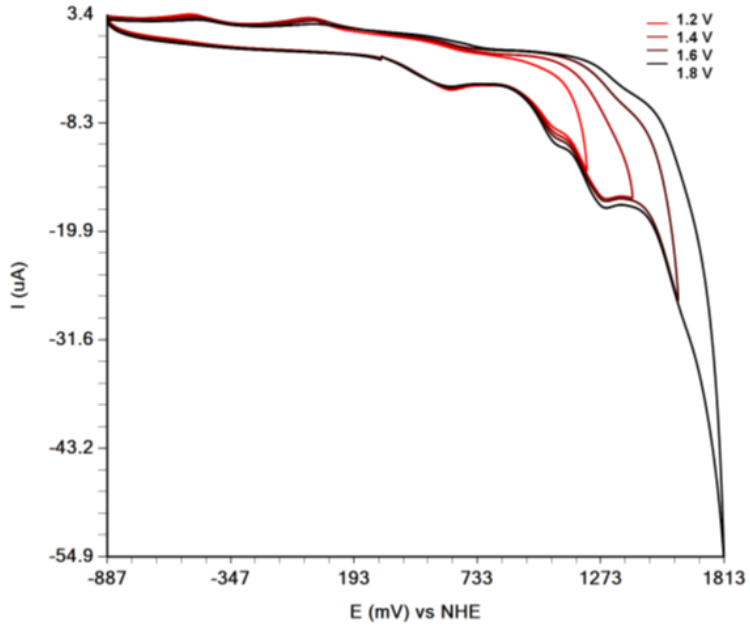

Fig. 12. CVs of the manganese(II) complex **1** (1 mM) in DMF containing water (20.0 mM) at different switching potentials . Scan rate 25mV/s.

In order to understand the mechanisms of the experimental voltammogram (Fig. 10), we simulated the CVs considering a simplified model of three redox reactions of the species s1, s2, s3 (s3 = Htrip, s1 and s2 the oxidized species of Htrip at approximately 1.15 and 1.33 V respectively, s4, s5 (s5=H_2O and s4 oxidised H_2O species) and the chemical reactions of the species s4 (conversion of s4 to s6 = O_2) and of the reactions of s5 with s1 and s2 to give s4. To successfully simulate the large decrease of the ligand's oxidation peaks current upon gradual addition of H_2O to the DMF solution of **1** we had to consider a fast reaction of the ligand's oxidized species s2 and s3 with s5 (H_2O). In addition, the simulated spectra (Fig. 13) show the same shift for the peaks at 1.155 and 1.326 V with the addition of s5 as in the experimental data (Fig. 10).

Experimental and simulation data clearly reveal that the free and the bound to the manganese complex oxidized ligand oxidizes H_2O to O_2. The Mn^{II} complexes are more effective in oxidizing H_2O than the free ligand (Fig. 9). This might be due to the higher thermodynamic stability of the ligand $trip^-$ in **1**-**3** in comparison with Htrip.

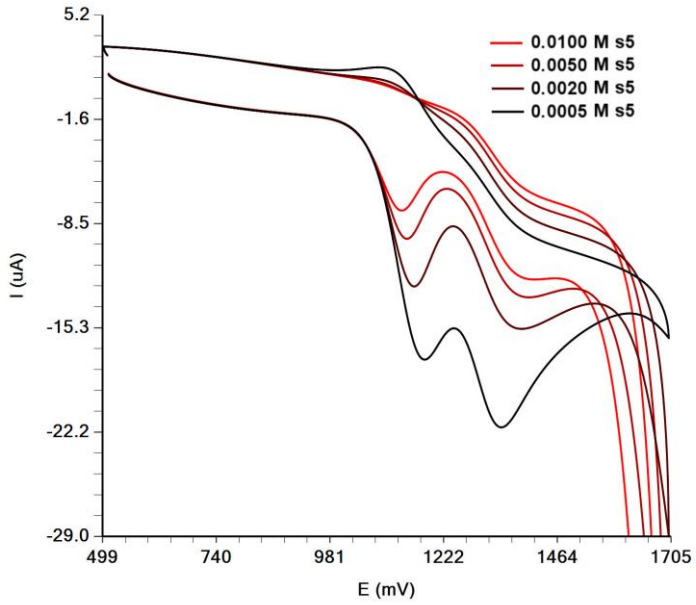

Fig. 13. Simulated voltammograms considering three electrochemical and three chemical reactions. s2 + 1e -> s1 E= 1.326 V, s1 + 1e -> s3 E= 1.155 V, s4 + 1e -> s5 E= 1.75 V, s4 ->

s6 k= 0.5 s^{-1}, s1 + s5 -> s4 k= 500 $^{s-1}$, s2 + s5 -> s4 k= 500 s^{-1}, E redox potentials and k rate constants. In the simulated spectra the concentration of s1 was 0.001 M and the concentration of s5 ranged from 0.0005 to 0.010 M.

3.5 UV-vis spectroscopy.

The UV-vis spectra of **1** and **2** in CH_2Cl_2 are shown in Fig. 14. In Table 4 are depicted the peaks with the absorption coefficients of **1**, **2**, and **3**. All complexes show a peak in the UV region assigned to the intra-ligand and ligand to metal electronic transitions. The absorption obeys the Lambert-Beer law for various concentrations of the complexes suggesting that the complexes remain stable in both CH_2Cl_2 and DMF solutions. In addition, the stability of the DMF solutions of the complexes after the addition of H_2O were also examined by UV-Vis. The UV-Vis spectra of the complexes were identical in 0 and 10% of H_2O/DMF solutions suggesting the complexes remain intact at these conditions (Fig. S8).

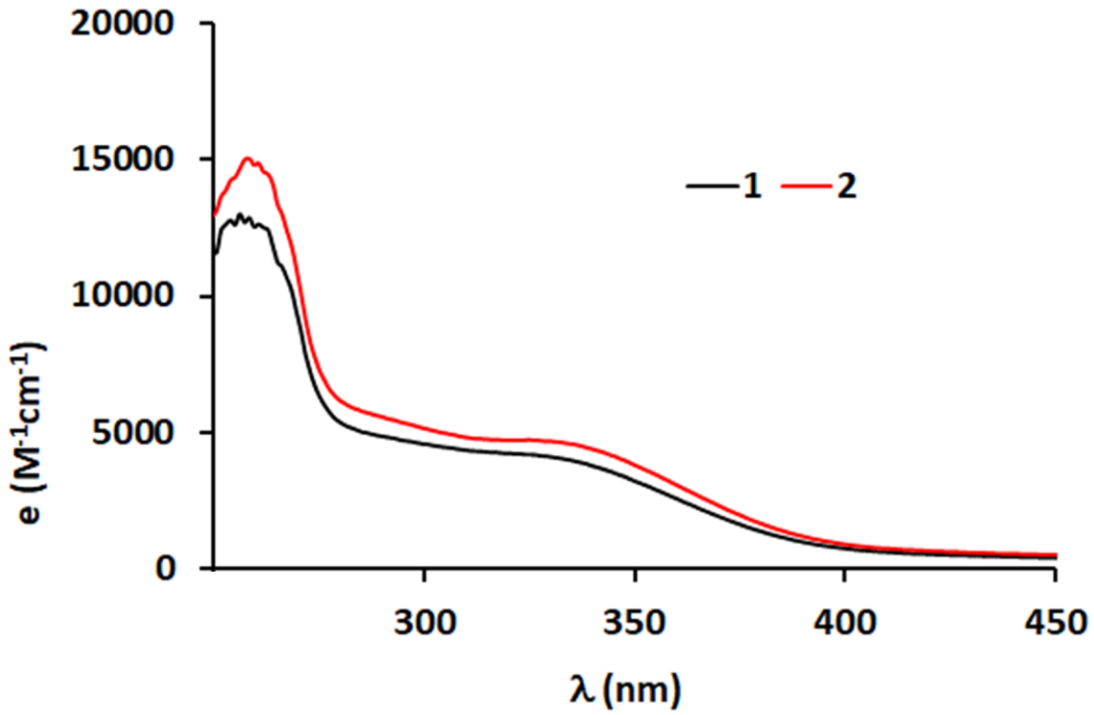

Fig. 14. UV-Vis spectra of **1** and **2** in CH_2Cl_2.

Table 4 The peaks and the absorption coefficients of **1**, **2**, and **3**.

Compound	**CH_2Cl_2** λ/nm (ε/$M^{-1}cm^{-1}$)	**DMF** λ/nm (ε/$M^{-1}cm^{-1}$)
1	327 (4290)	344 (3010)
2	333 (4580)	347 (3100)
3	-	401(124), 287(3812)

4. Conclusion

In conclusion, three manganese(II) complexes with the new *N*5 tripodal-amidate ligand Htrip were synthesized, structurally and physicochemically characterized. These complexes constitute the first mononuclear Mn^{II} high-spin complexes of the general formula $\{Mn^{II}(N5_{trip})X\}$ to be reported. Single crystal X-ray structure analysis revealed that the manganese(II) atom in **1-3** occupies the center of a severely distorted octahedron.

Cyclic voltametric study of compounds **1-3** revealed an unusual two electron-oxidation of Mn^{II} to Mn^{IV}. Electrochemical studies showed that the addition of H_2O to the DMF solutions of the Mn(II)-trip complexes **1-3** reveals electrochemically a thermodynamic stabilization of the ligand towards oxidation. The experimental and simulated data show that this ligand stabilization is done at the expense of H_2O. This indirect oxidation of H_2O from the oxidized ligand bound to Mn^{II} complexes define a new strategy to overcome the ligands instability of the metallorganic H_2O oxidation catalysts.

Efforts to isolate and further characterize the Mn^{IV} species and investigate its properties towards the oxidation of organic substrates are underway.

Acknowledgements

The research work was supported by the Hellenic Foundation for Research and Innovation (HFRI) under the HFRI PhD Fellowship grant (Fellowship Number: 1213). The authors wish to thank Assistant Professor Dr. Angelos G. Kalampounias, Department of Chemistry, University of Ioannina for helping in recording FTIR spectra and the university of Glasgow for supporting this work. The Single-Crystal X-ray Diffraction Unit of the Network of Research Supporting Laboratories, University of Ioannina, financed by the Regional Operational Programme (ROP) of the Epirus Region General Secretariat is also acknowledged.

Appendix A. Supplementary data

CCDC 2067257, 2067258 and 2067259 contains the supplementary crystallographic data for **1**, **2** and, **3** respectively. These data can be obtained free of charge via http://www.ccdc.cam.ac.uk/conts/retrieving.html, or from the Cambridge Crystallographic

Data Centre, 12 Union Road, Cambridge CB2 1EZ, UK; fax: (+44) 1223-336-033; or e-mail: deposit@ccdc.cam.ac.uk. Supplementary data associated with this article can be found, in the online version, at …

References

[1] (a) Frausto da Silva, J. J. R.; Williams, R. J. P. The Biological Chemistry of Elements. The Inorganic Chemistry of Life; Clarendon Press: Oxford, England (1991). (b) Cotton, F. A.; Wilkinson, G. Advanced Inorganic Chemistry; John Wiley & Sons: New York (1988)

[2] S. Signorella, C. Palopoli, G. Ledesma, Rationally designed mimics of antioxidant manganoenzymes: Role of structural features in the quest for catalysts with catalase and superoxide dismutase activity, Coord. Chem. Rev. 365 (2018) 75.

[3] (a) H. B. Lee, A. A. Shiau, P. H. Oyala, D. A. Marchiori, S. Gul, R. Chatterjee, J. Yano, R. D. Britt, T. Agapie, Tetranuclear [$Mn^{III}Mn_3^{IV}O_4$] Complexes as Spectroscopic Models of the S2 State of the Oxygen Evolving Complex in Photosystem II, J. Am. Chem. Soc. 140 (2018) 17175. (b) V. Krewald, M. Retegan, N. Cox, J. Messinger, W. Lubitz, S. DeBeer, F. Neese, D. A. Pantazis, Metal oxidation states in biological water splitting, Chem. Sci. 6 (2015) 1676. (c) L. Rapatskiy, N. Cox, A. Savitsky, W. M. Ames, J. Sander, M. M. Nowaczyk, M. Rogner, A. Boussac, F. Neese, J. Messinger, W. Lubitz, Detection of the Water-Binding Sites of the Oxygen-Evolving Complex of Photosystem II Using W-Band 17O Electron–Electron Double Resonance-Detected NMR Spectroscopy, J. Am. Chem. Soc.134 (2012) 16619. (d) B. Gerey, E. Goure, J. Fortage, J. Pecaut and M.-N. Collomb, Manganese-calcium/strontium heterometallic compounds and their relevance for the oxygen-evolving center of photosystem II, Coord. Chem. Rev. 319 (2016) 1. (e) S. Mukherjee, J. A. Stull, J. Yano, T. C. Stamatatos, K. Pringouri, T. A. Stich, K. A. Abboud, R. D. Britt, V. K. Yachandra and G. Christou, Synthetic model of the asymmetric [Mn_3CaO_4] cubane core of the oxygen-evolving complex of photosystem II, PNAS, 109 (2012) 2257−2262.

[4] (a) R. D. Cannon and R. P. White, Chemical and Physical Properties of Triangular Bridged Metal Complexes, Prog. Inorg. Chem. 36 (1988) 195. (b) G. Maayan, N. Gluz and G. Christou, A bioinspired soluble manganese cluster as a water oxidation electrocatalyst with low overpotential, Nat. Catal. 1 (2018) 48. (c) J. D. Parham, G. B. Wijeratne, D. B. Rice and T. A. Jackson, Spectroscopic and Structural Characterization

of Mn(III)-Alkylperoxo Complexes Supported by Pentadentate Amide-Containing Ligands, Inorg. Chem. 57 (2018) 2489.

[5] X. Chai, H. Huang, H. Liu, Z. Ke, W. Yong, M.T. Zhang, Y. S. Cheng, X. Wei, L. Zhanga, G. Yuan, Highly efficient and selective photocatalytic CO2 to CO conversion in aqueous solution, Chem. Commun. 56 (2020) 3851

[6] R. L. Shook, A. S. Borovik, Role of the Secondary Coordination Sphere in Metal-Mediated Dioxygen Activation, Inorg. Chem. 49 (2010) 3646–3660

[7] D, Bansal, G. Kumar, G. Hundal, R. Gupta, Mononuclear complexes of amide-based ligands containing appended functional groups: role of secondary coordination spheres on catalysis, Dalton Trans. 43 (2014) 14865

[8] (a) D.S Marlin, P.K. Mascharak, Coordination of carboxamido nitrogen to tervalent iron: insight into a new chapter of iron chemistry, Chem. Soc. Rev. 29 (2000) 69. (b) D.S. Marlin, M.M. Olmstead, P.K. Mascharak, Carboxamido Nitrogens Are Good Donors for Fe(III): Syntheses, Structures, and Properties of Two Low-Spin Nonmacrocyclic Iron(III) Complexes with Tetracarboxamido-N Coordination, Inorg. Chem. 38 (1999) 3258.

[9] (a) J. Lin,C. Tu, H. Lin, P. Jiang, J. Ding, Z. Guo, Crystal structure and superoxide dismutase activity of a six-coordinate manganese(III) complex, Inorg. Chem. Commun. 6 (2003) 262. (b) R.F Moreira, P.M. When, D. Sames, Highly Regioselective Oxygenation of C-H Bonds: Diamidomanganese Constructs with Attached Substrates as Catalyst Models Angew. Chem., Int. Ed. 39 (2000) 1618. (c) C.-M. Che, W.-K. Cheng, J. Chem. Soc., Manganese(III) amide complexes as a new class of catalyst for efficient alkene epoxidation Chem. Commun. (1986) 1443.

[10] (a) S.K. Chandra, A. Chakravorty, Two manganese(IV) complexes with isomeric MnN4O2 spheres incorporating hexadentate amide-amine-phenolate coordination, Inorg. Chem. 31 (1992) 474. (b) S.K. Chandra, S.B. Choudhury, D. Ray, A. Chakravorty, J. Chem. Soc. Chem. Commun., Manganese(IV)–amide binding: structural characterisation and redox stability of a hexadentate complex, (1990)474.

[11] (a) F.M MacDonnell, N.L.P Fackler, C. Stern, T.V. O'Halloran, Air Oxidation of a Five-Coordinate Mn(III) Dimer to a High-Valent Oxomanganese(V) Complex, J. Am. Chem. Soc. 116 (1994) 7431. (b) T.J. Collins, R.D. Powell, C. Slebodnick, E.S Uffelman, A water-stable manganese(V)-oxo complex: definitive assignment of a .nu.Mnv.tplbond.O infrared vibration, J. Am. Chem. Soc. 112 (1990) 899.

[12] G. Parkin, The bioinorganic chemistry of zinc: synthetic analogues of zinc enzymes that feature tripodal ligands, Chem Commun, (2000) 1971

[13] (a) Y. Hitomi, A. Ando, H. Matsui, T. Ito, T. Tanaka, S. Ogo, T. Funabiki, Aerobic catechol oxidation catalyzed by a bis(μ-oxo)dimanganese(III,III) complex via a manganese(II)-semiquinonate complex, Inorg Chem. 44 (2005) 3473–3478. (b) T. Nagataki, K. Ishii, Y. Tachi, S. Itoh, Ligand effects on NiII-catalysed alkane-hydroxylation with m-CPBA, Dalton Trans. (2007) 1120–1128. (c) R. Mas-Ballesté, L Que Jr., Iron-Catalyzed Olefin Epoxidation in the Presence of Acetic Acid: Insights into the Nature of the Metal-Based Oxidant, J. Am. Chem Soc. 129 (2007) 15964–15972.

[14] (a) Z. Dai, JW. Canary, Tailoring tripodal ligands for zinc sensing, New J. Chem. 31 (2007) 1708–1718. (b) ME Masaki, D. Paul, R. Nakamura, Y. Kataoka, S. Shinoda, H. Tsukube, Chiral tripode approach toward multiple anion sensing with lanthanide complexes, Tetrahedron. 65 (2009) 2525–2530.

[15] (a) C. Chiueh, J.-S. Hong, S.K. Leong, Nitric Oxide: Novel Actions, Deleterious Effects, and Clinical Potential; New York Academy of Sciences: New York (2002) p 962. (b) L.J. Ignarro, Nitric Oxide: Biology and Pathology Ed.; Academic Press: San Diego (2000). (c) J. Lincoln, G. Burnstock, Nitric Oxide in Health and Disease; Cambridge University Press: New York (1997)

[16] (a) A.-M. Simeone, S. Collela, R. Krahe, M.M Johnson, E. Mora, A.M. Tari, N-(4-Hydroxyphenyl)retinamide and nitric oxide pro-drugs exhibit apoptotic and anti-invasive effects against bone metastatic breast cancer cells, Carcinogenesis 27 (2006) 568-577.

[17] (a) D. Natale and J. C. Mareque-Rivas, The combination of transition metal ions and hydrogen-bonding interactions, Chem. Commun. (2008) 425; (b) R. L. Shook and A. S. Borovik, The effects of hydrogen bonds on metal-mediated O2activation and related processes, Chem. Commun., (2008) 6095; (c) L. Brammer, Metals and hydrogen bonds, Dalton Trans. (2003) 3145.

[18] (a) J. Yano and V. Yachandra, Mn4Ca Cluster in Photosynthesis: Where and How Water is Oxidized to Dioxygen, Chem. Rev. 114 (2014) 4175–4205. (b) K. Ogata, T. Yuki, M. Hatakeyama, W. Uchida and S. Nakamura, All-Atom Molecular Dynamics Simulation of Photosystem II Embedded in Thylakoid Membrane, J. Am. Chem. Soc. 135, (2013) 15670–15673 (c) J. Yang, D. Wang, H. Han, C. Li, Roles of Cocatalysts in Photocatalysis and Photoelectrocatalysis, Acc. Chem. Res. 46 (2013) 1900–1909.

[19] (a) N. S. Lewis, Toward Cost-Effective Solar Energy Use, Science 315 (2007) 798-801. (b) J. Barber, P. D. Tran, From natural to artificial photosynthesis, J. R. Soc. Interface, 10 (2003) 290. (c) I. McConnell, G. Li, G. W. Brudvig, Energy conversion in natural and artificial photosynthesis, Chem. Biol. 17 (2010) 434-447

[20] G. C. Dismukes, R. Brimblecombe, G. A. Felton, R. S. Pryadun, J. E. Sheats, L. Spiccia, and G. F. Swiegers, Development of bioinspired Mn4O4-cubane water oxidation catalysts: lessons from photosynthesis, Acc. Chem. Res. 42 (2009) 1935-1943

[21] (a) M. Yagi and K. Narita, Catalytic O_2 Evolution from Water Induced by Adsorption of $[(OH_2)(Terpy)Mn(\mu\text{-}O)_2Mn(Terpy)(OH_2)]^{3+}$ Complex onto Clay Compounds, J. Am. Chem. Soc. 126 (2004) 8084-8085. (b) W. F. Ruettinger, C. Campana and G. C. Dismukes, Synthesis and Characterization of Mn4O4L6 Complexes with Cubane-like Core Structure: A New Class of Models of the Active Site of the Photosynthetic Water Oxidase, J. Am. Chem. Soc. 119 (1997) 6670-6671. (c) Schwarz, B. et al., Visible-Light-Driven Water Oxidation by a Molecular Manganese Vanadium Oxide Cluster, Angew. Chem. Int. Ed. 55 (2016) 6329–6333. (d) N. Gluz, G. Christou and G. Maayan, The Role of the −OH Groups within Mn_{12} Clusters in Electrocatalytic Water Oxidation, Chem. Eur. J. 27 (2021) 6034 -6043. (e) W.-T. Lee, S. B. Munoz, D. A. Dickie and J. M. Smith, Ligand Modification Transforms a Catalase Mimic into a Water Oxidation Catalyst, Angew. Chem. Int. Ed. 53 (2014) 9856–9859.

[22] D. Shaffer, Y. Xie and J. Concepcion, O–O bond formation in ruthenium-catalyzed water oxidation: single-site nucleophilic attack vs. O–O radical coupling, Chem. Soc. Rev. 46 (2017) 6170–6193.

[23] Bruker, APEX 3; SAINT, SHELXT. (2016) Bruker AXS Inc., 5465 East Cheryl Parkway, Madison, WI 53711.

[24] G. M. Sheldrick, (1996) SADABS. University of Göttingen, Germany.

[25] G. M. Sheldrick, Crystal structure refinement with SHELXL, Acta Cryst. C71 (2015) 3.

[26] C. B. Hübschle, G.M. Sheldrick, B. Dittrich, ShelXle: a Qt graphical user interface for SHELXL, J. Appl. Cryst. 44 (2011) 1281.

[27] A. L. Spek, Structure validation in chemical crystallography, Acta Cryst. D65 (2009) 148.

[28] Diamond - Crystal and Molecular Structure Visualization, Crystal Impact - Dr. H. Putz & Dr. K. Brandenburg GbR, Kreuzherrenstr. 102, 53227 Bonn, Germany, http://www.crystalimpact.com/diamond.

[29] C. R. Groom, I. J. Bruno, M. P. Lightfoot, S. C. Ward, The Cambridge Structural Database, Acta Cryst. B72 (2016) 171. CSD codes: AFEWOA, BIVDAN, BIVDER, BIVDIV, BIVDOB, BIWJUP, BIWKAW, BIWKEA, BIWKIE, CAZNEX, CAZNIB, CAZNOH, CAZNUN, ETEFAM, ETEFEQ, FIZQEL, FIZQIP, HOCREX, HOCRIB, IHEBOP, WIZXOE, WOZFAE, WOVXUC.

[30] Y. Hitomi, Y. Iwamoto, M. Kodera, Electronic tuning of nitric oxide release from manganese nitrosyl complexes by visible light irradiation: enhancement of nitric oxide release efficiency by the nitro-substituted quinoline ligand, Dalton Trans. 43 (2014) 2161.

[31] K. Ghosh, A. A. Eroy-Reveles, B. Avila, T. R. Holman, M. M. Olmstead, P. K. Mascharak, Reactions of NO with Mn(II) and Mn(III) centers coordinated to carboxamido nitrogen: synthesis of a manganese nitrosyl with photolabile NO, Inorg. Chem. 43 (2004) 2988.

[32] A. A. Eroy-Reveles, Y. Leung, C. M. Beavers, M. M. Olmstead, P. K. Mascharak, Near-infrared light activated release of nitric oxide from designed photoactive manganese nitrosyls: strategy, design, and potential as NO donors, J. Am. Chem. Soc. 130 (2008) 4447.

[33] D. B. Rice, G. B. Wijeratne, A. D. Burr, J. D. Parham, V. W. Day, T. A. Jackson, Steric and Electronic Influence on Proton-Coupled Electron-Transfer Reactivity of a Mononuclear Mn(III)-Hydroxo Complex, Inorg. Chem. 55 (2016) 8110.

[34] R. Ketkaew, Y. Tantirungrotechai, P. Harding, G. Chastanet, P. Guionneau, M. Marchivie, D.J. Harding, OctaDist: a tool for calculating distortion parameters in spin crossover and coordination complexes Dalton Trans. 50 (2021) 1086 and references cited therein.

[35] D. J. Barnes, R. L. Chapman, F. S. Stephens, R. S. Vagg, Studies on the metal-amide bond. VII. Metal complexes of the flexible N4 ligand N,N′-bis(2′-pyridinecarboxamide)1,2-ethane, Inorg. Chim. Acta. 51 (1981) 155-162.

[36] T. Kurahashi, A. Kikuchi, T. Tosha, Y. Shiro, T. Kitagawa and H. Fujii, Transient Intermediates from Mn(salen) with Sterically Hindered Mesityl Groups: Interconversion between MnIV-Phenolate and MnIII-Phenoxyl Radicals as an Origin for Unique Reactivity, Inorg. Chem. 47 (2008) 1674-1686

[37] M. K. Coggins, A. N. Downing, W. Kaminsky and J. A. Kovacs, Comparison of two $Mn^{IV}Mn^{IV}$-bis-l-oxo complexes $\{[Mn^{IV}(N_4(6\text{-Me-DPEN}))]_2(l\text{-}O)_2\}^{2+}$ and $\{[Mn^{IV}(N_4(6\text{-Me-DPPN}))]_2(l\text{-}O)_2\}^{2+}$, Acta Crystallogr. Sect. Sect. E: Struct. Commun. 76 (2020) 1042-1046.

[38] C. Herrero, A. Quaranta, S. Protti, W. Leibl, A. W. Rutherford, D. R. Fallahpour, M. F. Charlot and A. Aukauloo, Light-driven activation of the $[H_2O(terpy)Mn^{III}\text{-}\mu\text{-}(O_2)\text{-}Mn^{IV}(terpy)OH_2]$ unit in a chromophore-catalyst complex, Chemistry - An Asian Journal 6 (2011) 1335-1339.

[39] D. B. Rice, A. A. Massie and T. A. Jackson, Experimental and Multireference ab Initio Investigations of Hydrogen-Atom-Transfer Reactivity of a Mononuclear Mn^{IV}-oxo Complex, Inorg. Chem. 58 (2019) 13902-13916.

[40] S. Romain, C. Baffert, C. Duboc, J. C. Leprêtre, A. Deronzier and M. N. Collomb, Mononuclear Mn^{III} and Mn^{IV} bis-terpyridine complexes: Electrochemical formation and spectroscopic characterizations, Inorg. Chem. 48 (2009) 3125-3131.

[41] Kurahashi, T.; Kikuchi, A.; Tosha, T.; Shiro, Y.; Kitagawa, T.; Fujii, H. Transient intermediates from Mn(salen) with sterically hindered mesityl groups: Interconversion between Mn^{IV}-phenolate and Mn^{III}-phenoxyl radicals as an origin for unique reactivity. Inorg. Chem. 2008, 47 (5), 1674-1686.

[42] M. Stylianou, I. Hadjiadamou, C. Drouza, S. C. Hayes, E. Lariou, I. Tantis, P. Lianos, A. C. Tsipis and A. D. Keramidas, Synthesis of new photosensitive $H_2BBQ^{2+}[ZnCl_4]^{2-}$/[$(ZnCl)_2$(μ-BBH)] complexes, through selective oxidation of H_2O to H_2O_2, Dalton Trans. 46 (2017), 3688-3699.

[43] S. Mavrikis, S. C. Perry, P. K. Leung, L. Wang and C. Ponce De León, Recent Advances in Electrochemical Water Oxidation to Produce Hydrogen Peroxide: A Mechanistic Perspective, ACS Sustainable Chemistry and Engineering 9 (2021) 76-91.